Draft version December 25, 2014
Preprint typeset using LaTeX style emulateapj v. 5/2/11

arXiv:1412.7162v2 [astro-ph.GA] 24 Dec 2014

PRIMUS: EFFECT OF GALAXY ENVIRONMENT ON THE QUIESCENT FRACTION EVOLUTION AT $z< 0.8$

ChangHoon Hahn[1], Michael R. Blanton[1], John Moustakas[2], Alison L. Coil[3], Richard J. Cool[4], Daniel J. Eisenstein[5], Ramin A. Skibba[3] Kenneth C. Wong[6], Guangtun Zhu[7]

Draft version December 25, 2014

ABSTRACT

We investigate the effects of galaxy environment on the evolution of the quiescent fraction ($f_{\rm Q}$) from $z = 0.8$ to 0.0 using spectroscopic redshifts and multi-wavelength imaging data from the PRIsm MUlti-object Survey (PRIMUS) and the Sloan Digitial Sky Survey (SDSS). Our stellar mass limited galaxy sample consists of $\sim 14,000$ PRIMUS galaxies within $z = 0.2-0.8$ and $\sim 64,000$ SDSS galaxies within $z = 0.05 - 0.12$. We classify the galaxies as quiescent or star-forming based on an evolving specific star formation cut, and as low or high density environments based on fixed cylindrical aperture environment measurements on a volume-limited environment defining population. For quiescent and star-forming galaxies in low or high density environments, we examine the evolution of their stellar mass function (SMF). Then using the SMFs we compute $f_{\rm Q}(\mathcal{M}_*)$ and quantify its evolution within our redshift range. We find that the quiescent fraction is higher at higher masses and in denser environments. The quiescent fraction rises with cosmic time for all masses and environments. At a fiducial mass of $10^{10.5}M_\odot$, from $z \sim 0.7$ to 0.1, the quiescent fraction rises by 15% at the lowest environments and by 25% at the highest environments we measure. These results suggest that for a minority of galaxies their cessation of star formation is due to external influences on them. However, in the recent Universe a substantial fraction of the galaxies that cease forming stars do so due to internal processes.

Subject headings: cosmology: observations — galaxies: evolution — galaxies: groups — galaxies: star formation

1. INTRODUCTION

Galaxies, in their detailed properties, carry the imprints of their surroundings, with a strong dependence of the quiescent fraction of galaxies on their local environment (e.g. Hubble 1936; Oemler 1974; Dressler 1980; Hermit et al. 1996; Guzzo et al. 1997; for a recent review see Blanton & Moustakas 2009). The strength of this dependence is itself a strongly decreasing function of galaxy stellar mass; at the extreme, the lowest mass ($< 10^9\ M_\odot$) galaxies end their star formation only in dense regions, and never in isolation (Geha et al. 2012). These effects also vary with redshift at least in the densest clusters, as observed in the changing fraction of late-type spirals relative to the field, found in studies of the morphology-density relation (Dressler 1984; Fasano et al. 2000; Smith et al. 2005; Desai et al. 2007). Clearly understanding the properties of galaxies in the present-day universe requires a careful investigation of the role of environment, and how that role changes over time.

Nevertheless, the evolution of the role of environment is a relatively subtle effect and must be interpreted within the context of the evolving galaxy population. For instance, the most dramatic change in galaxy properties during the past eight billion years has been the remarkable decline in the star-formation rate of galaxies in the Universe (Hopkins & Beacom 2006). This decline appears dominated by decreases in the rates of star-formation of individual galaxies (Noeske et al. 2007). There is evidence that a large fraction of the decline is associated with strongly infrared-emitting starbursts (Bell et al. 2005; Magnelli et al. 2009). As Cooper et al. (2008) and others have pointed out, because the environmental dependence of total star-formation rates at fixed redshift is relatively small, environmental effects are unlikely to cause the overall star-formation rate decline.

During this period, the major classes of galaxies that we observe today have already been firmly in place (Bundy et al. 2006; Borch et al. 2006; Taylor et al. 2009; Moustakas et al. 2013). Though not as dramatic as the history of galaxies prior to $z \sim 1$, detailed observations of the stellar mass function find significant evolution of the galaxy population with the decline in the number density of massive star-forming galaxies accompanied by an increase in the number density of quiescent galaxies (Blanton et al. 2006; Bundy et al. 2006; Borch et al. 2006; Moustakas et al. 2013). Moustakas et al. (2013), for instance, find that since $z \sim 1.0$ the $\sim 50\%$ decline in the number density of massive star-forming galaxies ($\mathcal{M}_* > 10^{11}\mathcal{M}_\odot$) is complemented by the rise in number density of intermediate-mass quiescent galaxies ($\mathcal{M}_* \approx 10^{9.5} - 10^{10}\mathcal{M}_\odot$), by a factor of $2-3$, and massive quiescent galaxies ($\mathcal{M}_* > 10^{11}\mathcal{M}_\odot$

[1] Center for Cosmology and Particle Physics, Department of Physics, New York University, 4 Washington Place, New York, NY 10003; chh327@nyu.edu
[2] Department of Physics and Astronomy, Siena College, 515 Loudon Road, Loudonville, NY 12211
[3] Center for Astrophysics and Space Sciences, Department of Physics, University of California, 9500 Gilman Dr., La Jolla, CA 92093
[4] MMT Observatory, University of Arizona, 1540 E Second Street, Tucson AZ 85721
[5] Harvard-Smithsonian Center for Astrophysics, 60 Garden Street, Cambridge, MA 02138
[6] Steward Observatory, University of Arizona, 933 North Cherry Avenue, Tucson, AZ 85721
[7] Hubble Fellow; Department of Physics and Astronomy, The Johns Hopkins University, 3400 North Charles Street, Baltimore, MD 21218

), by $\sim 20\%$. On the color-magnitude diagram, this corresponds to the doubling of the red sequence over this period (Bell et al. 2004; Borch et al. 2006; Faber et al. 2007). These changes in galaxy population are likely a result of physical processes that cause the cessation of star-formation in star-forming galaxies.

Of the numerous mechanisms that have been proposed to explain this cessation, favored models suggest that internal processes such as supernovae or active galactic nuclei heat the gas within the galaxy, which consequently suppresses the cold gas supply used for star-formation (Kereš et al. 2005; Croton et al. 2006; Dekel & Birnboim 2008). Other models propose that environment dependent external processes such as ram-pressure stripping (Gunn & Gott 1972; Bekki 2009), strangulation (Larson et al. 1980; Balogh et al. 2000), or harassment (Moore et al. 1998) contribute to the cessation.

Observations such as Weinmann et al. (2006) and Peng et al. (2010) credit some of these proposed internal processes for the cessation of star-formation, especially in massive galaxies. Meanwhile, observations of galaxy properties such as color and morphology correlating with environment suggest that environment may play a role in ceasing star-formation (Blanton & Moustakas 2009 and references therein). However, it remains to be determined whether the environmental trends in galaxy properties reflect the direct effect of external environment on the galaxies' evolution (e.g. ram pressure, tidal forces, mergers) or reflect statistical differences in the histories of galaxies in different environments (e.g. an earlier formation time in dense regions).

In this paper we take the most straightforward investigation by directly determining the star-forming properties of galaxies as a function of environment, stellar mass and redshift in a single, consistently analyzed data set. This analysis can reveal how galaxies end their star formation over time, quantitatively establish the contribution of environmental effects to the overall trends, and reveal whether those trends happen equally in all environments. However, such an analysis has not been done previously due to the lack of sufficiently large samples. In this paper, we apply this approach using the PRIism MUlti-object Survey (PRIMUS; Coil et al. 2011, Cool et al. 2013), the largest available redshift survey covering the epochs between $0 < z < 1$.

In Section 2 we present a brief description of the PRIMUS and SDSS data, our mass complete sample construction, and galaxy environment measurements. After dividing our galaxy sample into subsamples of star-forming or quiescent and high or low density environments, we compute and examine the evolution of the stellar mass functions for our subsamples in Section 3. In Section 4, we calculate the quiescent fraction, analyze the evolution of the quiescent fraction, quantify the effects of environment on the quiescent fraction evolution, and discuss the implications of our quiescent fraction results on the cessation of star-formation in galaxies. Finally in Section 5 we summarize our results.

Throughout the paper we assume a cosmology with $\Omega_m = 0.3, \Omega_\Lambda = 0.7$, and $H_0 = 70$ km s^{-1}Mpc^{-1}. All magnitudes are AB-relative.

2. SAMPLE SELECTION

We are interested in quantifying the effects of galaxy environment on the evolution of the quiescent fraction over the redshift range $0 < z < 1$. For our analysis, we require a sample with sufficient depth and high quality spectroscopic redshift to probe the redshift range and to robustly measure galaxy environment. PRIMUS with its $\sim 120,000$ spectroscopic redshifts provides a large data set at intermediate redshifts for our analysis. In addition, we anchor our analysis with a low redshift sample derived from the Sloan Digital Sky Survey (York et al. 2000).

In Section 2.1 and Section 2.2 we provide a brief summary of the PRIMUS and SDSS data used for our sample selection. In Section 2.3 we define our stellar mass complete galaxy sample. Then, in Section 2.4, we classify the sample galaxies as quiescent or star-forming. We calculate the environment using a volume-limited Environment Defining Population in Section 2.5. Finally, in Section 2.6, we account for edge effects in the surveys.

2.1. *PRIMUS*

At intermediate redshifts we use multiwavelength imaging and spectroscopic redshifts from PRIMUS, a faint galaxy survey with $\sim 120,000$ redshifts ($\sigma_z/(1+z) \approx 0.5\%$) within the range $z \approx 0-1.2$. The survey was conducted using the IMACS spectrograph on the Magellan I Baade 6.5-m telescope with a slitmask and low dispersion prism. For details on the PRIMUS observation methods such as survey design, targeting, and data summary, we refer readers to the survey papers (Coil et al. 2011; Cool et al. 2013).

While the PRIMUS survey targeted seven distinct extragalactic deep fields for a total of ~ 9 deg^2, we restrict our sample to five fields that have *GALEX* and *Spitzer*/IRAC imaging for a total of ~ 5.5 deg^2 (similar to the sample selection in Moustakas et al. 2013). Four of these fields are a part of the *Spitzer* Wide-area Infrared Extragalactic Survey (SWIRE[8]): the European Large Area ISO Survey - South 1 field (ELAIS-S1[9]), the Chandra Deep Field South SWIRE field (CDFS), and the XMM Large Scale Structure Survey field (XMM-LSS). The XMM-LSS consists of two separate but spatially adjacent fields: the Subaru/XMM-Newton DEEP Survey field (XMM-SXDSS[10]) and the Canadian-France-Hawaii Telescope Legacy Survey field (XMM-CFHTLS[11]). Our fifth and final field is the Cosmic Evolution Survey (COSMOS[12]) field. For all of our fields we have near-UV (NUV) and far-UV (FUV) photometry from the *GALEX* Deep Imaging Survey (DIS; Martin et al. 2005; Morrissey et al. 2005) as well as ground-based optical and *Spitzer*/IRAC mid-infrared photometric catalogs. Moustakas et al. (2013) provides detailed descriptions of integrated flux calculations in the photometric bands for each of our fields. Furthermore, we derive the *K-corrections* from the photometry using `K-correct` (v4.2; Blanton & Roweis 2007).

Finally, using the spectroscopic redshift and broad wavelength photometry we apply `iSEDfit`, a Bayesian SED modeling code, to calculate stellar masses and star

[8] http://swire.ipac.caltech.edu/swire/swire.html
[9] http://dipastro.pd.astro.it/esis
[10] http://www.naoj.org/cience/SubaruProject/SDS
[11] http://www.cfht.hawaii.edu/Science/CFHLS
[12] http://cosmos.astro.caltech.edu

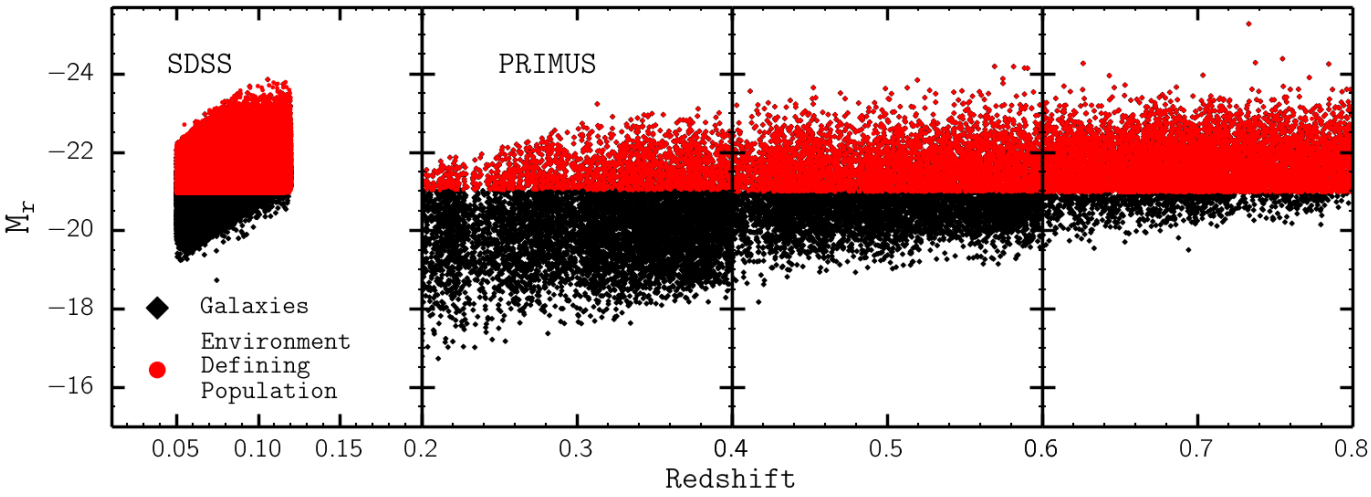

FIG. 1.— Absolute magnitude M_r versus redshift for our mass complete galaxy sample (black squares) with the Environment Defining Population (red circles) plotted on top. Both samples are divided into redshift bins: $z = 0.05 - 0.12$, $0.2 - 0.4$, $0.4 - 0.6$, and $0.6 - 0.8$ (panels left to right). The lowest redshift bin ($z \approx 0.05 - 0.12$; leftmost panel) contain our galaxy sample and EDP selected from SDSS. The rest contain galaxies and EDP selected from PRIMUS. The redshift limits for the lowest redshift bin are empirically selected based on the bright and faint limits of SDSS galaxies. Stellar mass completeness limits, described in Section 2.3, are imposed on the galaxy population. Meanwhile, M_r limits are applied to the EDP such that the number density in each panel are equivalent (Section 2.5).

formation rates (SFRs) for our sample galaxies (Moustakas et al. 2013). `iSEDfit` uses the redshift and the observed photometry of the galaxies to determine the statistical likelihood of a large ensemble of generated model SEDs. The model SEDs are generated using Flexible Stellar Population Synthesis (FSPS) models (Conroy & Gunn 2010) based on the Chabrier (2003) IMF, along with other prior parameters discussed in Section 4.1 and Appendix A of Moustakas et al. (2013). For the observed photometry, we use the *GALEX* FUV and NUV, the two shortest IRAC bands at 3.6 and 4.5μm (the two longer-wavelength IRAC channels are excluded because `iSEDfit` does not model hot dust or polycyclic aromatic hydrocarbons emission lines), and the optical bands.

2.2. *SDSS-GALEX*

At low redshifts, we use spectroscopic redshifts and *ugriz* photometry from the SDSS Data Release 7 (DR7; Abazajian et al. 2009). More specifically we select galaxies from the New York University Value-Added Galaxy Catalog (hereafter VAGC) that satisfy the main sample criterion and have galaxy extinction corrected Petrosian magnitudes $14.5 < r < 17.6$ and spectroscopic redshifts within $0.01 < z < 0.2$ (Blanton et al. 2005b). We further restrict the VAGC sample to only galaxies with medium depth observations with total exposure time greater than 1 ks from *GALEX* Release 6. This leaves 167, 727 galaxies.

Next, we use the MAST/CasJobs[13] interface and a 4″ diameter search radius, to obtain the NUV and FUV photometry for the SDSS-*GALEX* galaxies. For optical photometry, we use the *ugriz* bands from the SDSS `model` magnitudes scaled to the r-band `cmodel` magnitude. These photometric bands are then supplemented with integrated JHK_s magnitudes from the 2MASS Extended Source Catalog (XSC; Jarrett et al. 2000) and with photometry at 3.4 and 4.6μm from the WISE All-Sky Data Release[14]. Further details regarding the SDSS-*GALEX* sample photometry can be found in Section 2.4 of Moustakas et al. (2013). As previously done on the PRIMUS data in Section 2.1, we use `iSEDfit` to obtain the stellar masses and star formation rates for the SDSS-*GALEX* sample.

The SDSS-*GALEX* data discussed above is derived from the NYU-VAGC based on SDSS Data Release 7, using the standard SDSS photometric measurements. Several investigators have found that the background subtraction techniques used in the standard photometric catalogs introduce a size dependent bias in the galaxy fluxes and consequently stellar masses (West 2005; Blanton et al. 2005a; Lauer et al. 2007; Bernardi et al. 2007; Hyde & Bernardi 2009; West et al. 2010).

In order to quantify the effects of these photometric underestimations in our analysis, we tried replacing our SDSS fluxes in the *ugriz* band with *ugriz* fluxes from the NASA-Sloan Atlas (NSA) catalog, which incorporate the improved background subtraction presented in Blanton et al. (2011) and uses single-Seric fit fluxes rather than the standard SDSS `cmodel` fluxes. Using the ratio of the luminosity derived from the improved photometry over the luminosity derived from the standard NYU-VAGC photometry, we apply a preliminary correction to the stellar mass values obtained from `iSEDfit` assuming a consistent mass-to-light ratio. This mass correction leads to a significant increase in the stellar mass function for $\mathcal{M} > 10^{11}\mathcal{M}_{\odot}$; however, the effect of the mass correction was negligible for the quiescent fraction evolution results. As a result, for the results presented here we use the standard SDSS fluxes and we do not discuss the issues with photometric measurements any further in this paper. We note that a thorough investigation of these issues to understand their effect on the stellar mass function requires a reanalysis of both the SDSS photometry

[13] http://galex.stsci.edu/casjobs

[14] http://wise2.ipac.caltech.edu/docs/release/allsky

and the deeper photometry used for PRIMUS targeting.

2.3. *Stellar Mass Complete Galaxy Sample*

From the low redshift SDSS-*GALEX* and intermediate redshift PRIMUS data we define our mass complete galaxy sample. We begin by imposing the parent sample selection criteria from Moustakas et al. (2013). More specifically, we take the statistically complete *primary* sample from the PRIMUS data (Coil et al. 2011) and impose magnitude limits on optical selection bands as specified in Moustakas et al. (2013) Table 1. These limits are in different optical selection bands and have distinct values for the five PRIMUS target fields. We then exclude stars and broad-line AGN to only select objects spectroscopically classified as galaxies, with high-quality spectroscopic redshifts ($Q \geq 3$). Lastly, we impose a redshift range of $0.2 < z < 0.8$ for the PRIMUS galaxy sample, where $z > 0.2$ is selected due to limitations from sample variance and $z < 0.8$ is selected due to the lack of sufficient statistics in subsamples defined below.

For the PRIMUS objects that meet the above criteria, we assign statistical weights (described in Coil et al. 2011 and Cool et al. 2013) in order to correct for targeting incompleteness and redshift failures. The statistical weight, w_i, for each galaxy is given by

$$w_i = (f_{\rm target} \times f_{\rm collision} \times f_{\rm success})^{-1}, \quad (1)$$

as in Equation (1) in Moustakas et al. (2013).

Since we are ultimately interested in a mass complete galaxy sample to derive SMFs and QFs, next we impose stellar mass completeness limits to our galaxy sample. Stellar mass completeness limits for a magnitude-limited survey such as PRIMUS are functions of redshift, the apparent magnitude limit of the survey, and the typical stellar mass-to-light ratio of galaxies near the flux limit. We use the same procedure as Moustakas et al. (2013), which follows Pozzetti et al. (2010), to empircally determine the stellar mass completeness limits. For each of the target galaxies we compute $\mathcal{M}_{\rm lim}$ using $\log\ \mathcal{M}_{\rm lim} = \log\ \mathcal{M} + 0.4\ (m - m_{\rm lim})$, where $\mathcal{M}$ is the stellar mass of the galaxy in $\mathcal{M}_\odot$, $\mathcal{M}_{\rm lim}$ is the stellar mass of each galaxy if its magnitude was equal to the survey magnitude limit, m is the observed apparent magnitude in the selection band, and $m_{\rm lim}$ is the magnitude limit for our five fields. We construct a cumulative distribution of $\mathcal{M}_{\rm lim}$ for the 15% faintest galaxies in $\Delta z = 0.04$ bins. In each of these redshift bins, we calculate the minimum stellar mass that includes 95% of the galaxies. Separately for quiescent and star-forming galaxies, we fit quadratic polynomials to the minimum stellar masses versus redshift (star-forming or quiescent classification is described in the following section). Finally, we use the polynomials to obtain the minimum stellar masses at the center of redshift bins, $0.2-0.4$, $0.4-0.6$, and $0.6-0.8$, which are then used as PRIMUS stellar mass completeness limits.

For the low redshift portion of our galaxy sample, we start by limiting the SDSS-*GALEX* data to objects within $0.05 < z < 0.12$, a redshift range later imposed on the volume-limited Environment Defining Population (Section 2.5). To account for the targeting incompleteness of the SDSS-*GALEX* sample, we use the statistical weight estimates provided by the NYU-VAGC catalog. Furthermore, we determine a uniform stellar mass completeness limit of $10^{10.2}\mathcal{M}_\odot$ above the stellar mass-to-light ratio completeness limit of the SDSS-*GALEX* data within the imposed redshift limits (Blanton et al. 2005a; Baldry et al. 2008; Moustakas et al. 2013). We then apply this mass limit in order to obtain our mass-complete galaxy sample at low redshift.

We now have a stellar mass complete sample derived from SDSS-*GALEX* and PRIMUS data. Since our sample is derived from two different surveys, we account for the disparity in the redshift uncertainty. While PRIMUS provides a large number of redshifts out to $z = 1$, due to its use of a low dispersion prism, the redshift uncertainties are significantly larger ($\sigma_z/(1+z) \approx 0.5\%$) than the uncertainties of the SDSS-*GALEX* redshifts. In order to have comparable environment measures throughout our redshift range, we apply PRIMUS redshift uncertainties to our galaxy sample selected from SDSS-*GALEX*. For each SDSS-*GALEX* galaxy, we adjust its redshift by randomly sampling a Gaussian distribution with standard deviation $\sigma = 0.005(1 + z_{\rm SDSS-GALEX})$, where $z_{\rm SDSS-GALEX}$ is the redshift of the galaxy.

2.4. *Classifying Quiescent and Star-Forming Galaxies*

We now classify our mass complete galaxy sample into quiescent or star-forming using an evolving cut based on specific star-formation rate utilized in Moustakas et al. (2013) Section 3.2. This classification method uses the star-forming (SF) sequence, which is the correlation between star-formation rate (SFR) and stellar mass in star-forming galaxies observed at least until $z \sim 2$ (Noeske et al. 2007; Williams et al. 2009; Karim et al. 2011). The PRIMUS sample displays a well-defined SF sequence within the redshift range of our galaxy sample. Using the power-law slope for the SF sequence from Salim et al. (2007) (SFR $\propto \mathcal{M}^{0.65}$) and the minimum of the quiescent/star-forming bimodality, determined empirically, we obtain the following equation to classify the target galaxies (Equation 2 in Moustakas et al. 2013):

$$\log({\rm SFR}_{\rm min}) = -0.49 + 0.64\log(\mathcal{M} - 10) + 1.07(z - 0.1), \quad (2)$$

where $\mathcal{M}$ is the stellar mass of the galaxy. If the target galaxy SFR and stellar mass lie above Equation 2 we classify it as star-forming; if below, as quiescent (Moustakas et al. 2013 Figure 1.).

2.5. *Galaxy Environment*

We define the environment of a galaxy as the number of neighboring Environment Defining Population galaxies (defined below) within a fixed aperture centered around it. We use fixed aperture measurements in order to quantify galaxy environment with an aperture sufficiently large to encompass massive halos (Muldrew et al. 2012; Skibba et al. 2013).

For our aperture, we use a cylinder of dimensions: $R_{\rm ap} = 2.5$ Mpc and $H_{\rm ap} = 35$ Mpc. We use a cylindrical aperture to account for the PRIMUS redshift errors and redshift space distortions (i.e. "Finger of God" effect). As Cooper et al. (2005) and Gallazzi et al. (2009) find, ± 1000 km s^{-1} optimally reduces the effects of redshift space distortions. The PRIMUS redshift uncertainty at $z \sim 0.7$ corresponds to $\sigma_z < 0.01$, so our choice of 35 Mpc for the aperture height accounts for both of these effects.

TABLE 1
GALAXY SUBSAMPLES

	$n_{\rm env}$	$N_{\rm gal}$		$\mathcal{M}_{\rm lim}$		$M_{\rm r,lim}$
		Quiescent	Star-Forming	Quiescent	Star-Forming	
$0.05 < z < 0.12$	$n_{\rm env} < 0.5$	6533	7508	$10^{10.2}\mathcal{M}_\odot$	$10^{10.2}\mathcal{M}_\odot$	-20.95
	$n_{\rm env} > 3.0$	14673	9717			
	all	33553	29864			
$0.2 < z < 0.4$	$n_{\rm env} < 0.5$	363	1231	$10^{9.8}\mathcal{M}_\odot$	$10^{9.8}\mathcal{M}_\odot$	-21.03
	$n_{\rm env} > 3.0$	379	756			
	all	1086	2879			
$0.4 < z < 0.6$	$n_{\rm env} < 0.5$	536	1498	$10^{10.3}\mathcal{M}_\odot$	$10^{10.3}\mathcal{M}_\odot$	-20.98
	$n_{\rm env} > 3.0$	490	854			
	all	1560	3577			
$0.6 < z < 0.8$	$n_{\rm env} < 0.5$	567	1254	$10^{10.7}\mathcal{M}_\odot$	$10^{10.6}\mathcal{M}_\odot$	-20.97
	$n_{\rm env} > 3.0$	498	671			
	all	1668	2964			
Total		77151				

Notes: Number of galaxies ($N_{\rm gal}$) in the mass complete subsamples within the edges of the survey (Section 2). The subsamples are classified based on environment ($n_{\rm env}$) and star formation rate (star-forming or quiescent). The lowest redshift bin is derived from SDSS; the rest are from PRIMUS. We also list the stellar mass completeness limit, $\mathcal{M}_{\rm lim}$, for our sample along with the r-band absolute magnitude limits, $M_{\rm r,lim}$, for the Environment Defining Population.

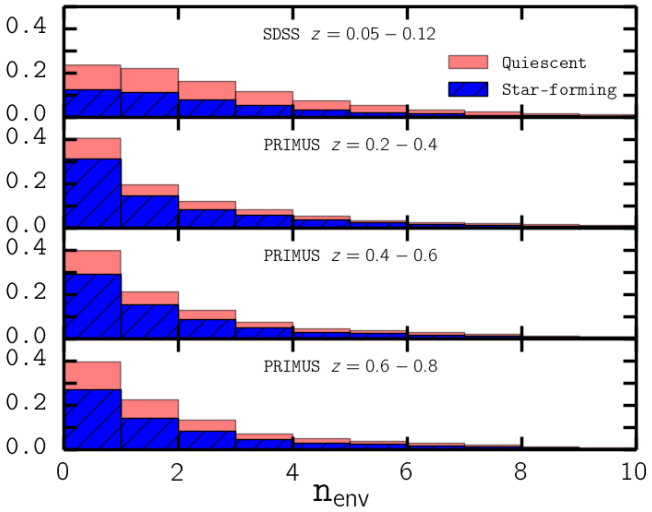

FIG. 2.— Normalized distribution of environment measurements ($n_{\rm env}$) for our mass complete galaxy sample within the survey edges. A fixed cylindrical aperture of $R_{\rm ap} = 2.5$ Mpc and $H_{\rm ap} = 35$ Mpc is used to measure environment. The star-forming galaxies contribution to the distribution is colored in blue and diagonally patterned. The contribution from quiescent galaxies is colored in red. Galaxies with $n_{\rm env} < 0.5$ are in low density environments and galaxies with $n_{\rm env} > 3.0$ are in high density environment. We note that the significant difference among the SDSS distribution and the PRIMUS distributions above is due to the different stellar mass completeness limits imposed on each redshift bin of our galaxy sample.

Our choice of cylinder radius was motivated by scale dependence analyses in the literature (Blanton et al. 2006; Wilman et al. 2010; Muldrew et al. 2012), which suggest that galactic properties such as color and quiescent fractions are most strongly dependent on scales < 2 Mpc, around the host dark matter halo sizes.

Before we measure the environment for our galaxy sample, we first construct a volume limited Environment Defining Population (EDP) with absolute magnitude cut-offs (M_r) in redshift bins with $\Delta z \sim 0.2$. The M_r cut-offs for the EDP are selected such that the cumulative number density over M_r for all redshift bins are equal. We make this choice in order to construct an EDP that contains similar galaxy populations through the redshift range (i.e. accounts for the progenitor bias). In their analysis of this method, Behroozi et al. (2013) and Leja et al. (2013) find that although it does not precisely account for the scatter in mass accretion or galaxy-galaxy mergers, it provides a reasonable means to compare galaxy populations over a wide range of cosmic time.

In constructing the PRIMUS EDP we use the same PRIMUS data used to select our galaxy sample (described in Section 2.3). We again restrict the PRIMUS galaxies to $0.2 < z < 0.8$ and divide them into bins of $\Delta z = 0.2$. Before we consider the cumulative number densities in the redshift bins, we first determine the M_r limit for the highest redshift bin ($z = 0.6 - 0.8$) by examining the M_r distribution with bin size $\Delta M_r = 0.25$ and select $M_{r,\rm lim}$ near the peak of the distribution where bins with $M_r > M_{r,\rm lim}$ have fewer galaxies than the bin at $M_{r,\rm lim}$. We conservatively choose $M_{r,\rm lim}(0.6 < z < 0.8)$ to be $M_r = -20.97$. Then for the lower redshift bins, we impose absolute magnitude limits ($M_{r,\rm lim}$) such that the cumulative number density, calculated with the galaxy statistical weights, of the bin ordered by M_r is equal to the cumulative number density of the highest redshift bin with $M_{r,\rm lim}(0.6 < z < 0.8) = -20.97$.

For the SDSS EDP, we do not use the SDSS-*GALEX* parent data, which is limited to the combined angular selection window of the VAGC and *GALEX* (Section 2.2). Instead, since FUV, NUV values are not necessary for the EDP, we extend the parent data of the SDSS EDP to the entire NYU-VAGC, including galaxies outside of the *GALEX* window function. Furthermore, we impose a redshift range of $0.05 - 0.12$ on the SDSS EDP. This redshift range was determined to account for the lack of faint galaxies at $z \sim 0.2$ and the lack of bright galaxies at $z \sim 0.01$ in the VAGC. As with the PRIMUS redshift

bins, we determine the SDSS EDP $M_{r,\rm lim}$ by matching the cumulative number density of the highest redshift bin. For redshift bins $z = 0.05-0.12$, $0.2-0.4$, $0.4-0.6$, $0.6-0.8$ we get $M_{r,\rm lim} = -20.95$, -21.03, -20.98 and -20.97, respectively. These absolute magnitude limits are illustrated in Figure 1, where we present the absolute magnitude (M_r) versus redshift for the galaxy sample (black squares) ad the EDP (red circles). The leftmost panel corresponds to the samples derived from the SDSS-*GALEX* data while the rest correspond to samples derived from the PRIMUS data divided in bins with $\Delta z \sim 0.2$. Figure 1 shows clear M_r cutoffs in the M_r distribution versus redshift for the EDP on top of our galaxy sample.

For our SDSS-*GALEX* galaxy sample, in Section 2.3, we apply PRIMUS redshift errors in order to establish a consistent measurement of environment throughout our redshift range. We appropriately apply equivalent redshift adjustments for the SDSS EDP. For the SDSS EDP galaxies that are also contained within the SDSS-*GALEX* sample, we adjust the redshift by an identical amount. For the rest, we apply the same redshift adjustment procedure described in Section 2.3 in order to obtain PRIMUS level redshift uncertainties.

Finally, we measure the environment for each galaxy in our galaxy sample by counting the number of EDP galaxies, $n_{\rm env}$, with RA, Dec, and z within our cylindrical aperture centered around it. $n_{\rm env}$ accounts for the statistical weights of the EDP galaxies. For our galaxy sample, the expected $n_{\rm env}$ given the uniform number density in each of our EDP redshift bin and volume of our cylindrical aperture is $\langle n_{\rm env}\rangle = 1.3$. Once we obtain environment measurements for all the galaxies in our galaxy sample, we classify galaxies with $n_{\rm env} < 0.5$ to be in "low" environment densities and galaxies with $n_{\rm env} > 3$ to be in "high" environment densities. The high environment cutoff was selected in order to reduce contamination from galaxies in low environment densities while maintaining sufficient statistics. In Section 4.2 we will also explore higher density cutoffs for $n_{\rm env}$.

The analysis we describe below uses a fixed cylindrical aperture with dimensions $R_{\rm ap} = 2.5$ Mpc and $H_{\rm ap} = 35$ Mpc to measure environment. The same analysis was extended for varying aperture dimensions $R_{\rm ap} = 1.5$, 2.5, 3.0 Mpc and $H_{\rm ap} = 35$, 70 Mpc with adjusted environment classifications. The results obtained from using different apertures and environment classifications are qualitatively consistent with the results presented below.

2.6. *Edge Effects*

One of the challenges in obtaining accurate galaxy environments using a fixed aperture method is accounting for the edges of the survey. For galaxies located near the edge of the survey, part of the fixed aperture encompassing it will lie outside the survey regions. In this scenario, n_{env} only reflects the fraction of the environment within the survey geometry.

To account for these edge effects, we use a Monte Carlo method to impose edge cutoffs on our galaxy sample. First, using `ransack` from Swanson et al. (2008), we construct a random sample of $N_{\rm ransack} = 1,000,000$ points with RA and Dec randomly selected within the window function of the EDP (SDSS EDP and PRIMUS EDP separately). We then compute the angular separation, $\theta_{i,\rm ap}$ that corresponds to $R_{\rm ap}$ (Section 2.5) at the redshift of each sample galaxy i. For each sample galaxy we count the number of `ransack` points within $\theta_{i,\rm ap}$ of the galaxy: $n_{i,\rm ransack}$. Afterwards, we compare $n_{i,\rm ransack}$ to the expected value computed from the angular area of the environment defining aperture and the EDP window function:

$$\langle n_{\rm ransack}\rangle_i = \frac{N_{\rm ransack}}{A_{\rm EDP}} \times \pi\theta_{i,\rm ap}^2 \times f_{\rm thresh}. \qquad (3)$$

$A_{\rm EDP}$ is the total angular area of the EDP window function and $f_{\rm thresh}$ is the fractional threshold for the edge effect cut-off. For $R_{\rm ap} = 2.5$ Mpc, we use $f_{\rm thresh} = 0.75$. If $n_{i,\rm ransack} > \langle n_{\rm ransack}\rangle_i$ then galaxy i remains in our sample; otherwise, it is discarded. Once the edge effect cuts are applied, we are left with the final galaxy sample. For our SDSS-*GALEX* galaxy sample, $\sim 12\%$ of galaxies are removed from the edge effect cuts. For our PRIMUS galaxy sample, $\sim 40\%$ of galaxies are removed from the edge effect cuts.

In Figure 2 we present the distribution of environment measurements ($n_{\rm env}$) for our final galaxy sample in redshift bins: $z = 0.05-0.12$, $0.2-0.4$, $0.4-0.6$, and $0.6-0.8$. The quiescent galaxy contributions are colored in red while the star-forming galaxy contributions are colored in blue and patterned. We classify galaxies with $n_{\rm env} < 0.5$ to be in low density environments and galaxies with $n_{\rm env} > 3.0$ to be in high density environments.

Although we imposed PRIMUS redshift errors on our SDSS galaxies to consistently measure environment throughout our entire sample, we note a significant discrepancy between the $n_{\rm env}$ distributions of the SDSS and PRIMUS samples. For example, in each of the PRIMUS redshift bins, $\sim 40\%$ of galaxies in the redshift bin are in low density environments and roughly 30% are in high density environments. In contrast, in the SDSS redshift bin, $\sim$ 20% of galaxies in the redshift bin are in low density environments and $\sim 35\%$ are in high density environments. We remind the reader that this is mainly due to the varying stellar mass-completeness limits imposed on our galaxy sample for each redshift bins and does not affect our results.

3. RESULTS: STELLAR MASS FUNCTION

Our galaxy sample has so far been classified into quiescent or star-forming and low or high density environments. We further divide these subsamples into redshift bins: $0.05-0.12$, $0.2-0.4$, $0.4-0.6$, and $0.6-0.8$ for a total of 16 subsamples. In Section 3.1, we calculate the SMF for each of these subsamples. Then we examine the evolution of active and quiescent subsample SMFs in different environments in Section 3.2.

3.1. *Stellar Mass Function Calculations*

To calculate the SMFs we employ a non-parametric $1/V_{\rm max}$ estimator commonly used for galaxy luminosity functions and stellar mass functions in order to account for Malmquist bias, as done in Moustakas et al. (2013) and discussed in the review Johnston (2011). The differential SMF is given by the following equation:

$$\Phi(\log \mathcal{M})\Delta(\log \mathcal{M}) = \sum_{i=1}^{N} \frac{w_i}{V_{\rm max,avail,}i}. \qquad (4)$$

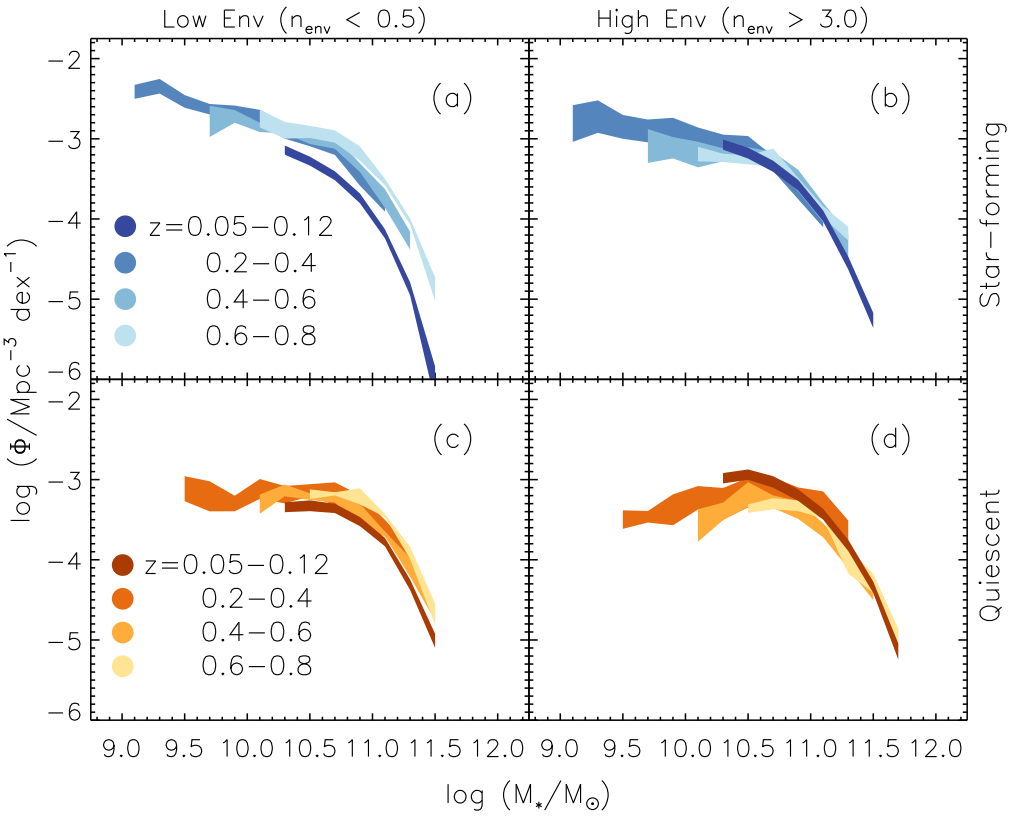

FIG. 3.— Evolution of stellar mass functions of star-forming (top) and quiescent (bottom) galaxies in low (left) and high (right) density environments throughout the redshift range $z = 0$–0.8. The environment of each galaxy was calculated using a cylindrical aperture size of $R = 2.5$ Mpc and $H = 35$ Mpc and classified as low environment when $n_{\rm env} < 0.5$ and as high environment when $n_{\rm env} > 3.0$. The SMFs use mass bins of width $\Delta\log(\mathcal{M}/\mathcal{M}_\odot) = 0.2$. In each panel we use shades of blue (star-forming) and orange (quiescent) to represent the SMF at different redshift, higher redshifts being progressively lighter.

w_i is the statistical weight of galaxy i and $\Phi(\log\,\mathcal{M})\Delta(\log\,\mathcal{M})$ is the number of galaxies (N) per unit volume within the stellar mass range $[\log\mathcal{M},\ \log\mathcal{M} + \Delta(\log\mathcal{M})]$. The equation above is the same as Equation 3 in Moustakas et al. (2013) except that we use $V_{\rm max,avail}$ instead than $V_{\rm max}$, to account for the edge effects of the survey discussed in Section 2.6.

$V_{{\rm max},i}$ is the maximum cosmological volume where it is possible to observe galaxy i given the apparent magnitude limits of the survey. However in Section 2.6 we remove galaxies that lie on the survey edges from our sample. In doing so, we reduce the maximum cosmological volume where a galaxy can be observed, thereby reducing the fraction of $V_{{\rm max},i}$ that is actually available in the sample. We introduce the term $V_{{\rm max,avail},i}$ to express the maximum volume accounting for the survey edge effects.

To calculate $V_{{\rm max,avail},i}$, we use a similar Monte Carlo method as the edge effect cutoffs in Section 2.6. First, we generate a sample of points with random RA, Dec within the window function of our galaxy sample (SDSS-*GALEX* window function and the five PRIMUS fields) and random z within the redshift range. These points are not to be confused with the `ransack` sample in Section 2.6. We apply the edge effect cuts on these random points as we did for our galaxy sample using the same method as in Section 2.6. Within redshift bins of $\Delta z \sim 0.01$, we calculate the fraction of the random points that remain in the bin after the edge effect cuts over the total number of random points in the bin: $f_{\rm edge}$. We then apply this factor to compute $V_{\rm max,avail} = V_{\rm max} \times f_{\rm edge}$. The $V_{\rm max}$ values in the equation above are computed following the method described in Moustakas et al. (2013) Section 4.2 with the same redshift-dependent K-correction from the observed SED and luminosity evolution model.

To calculate the uncertainty of the SMFs from the sample variance, we use a standard jackknife technique (following Moustakas et al. 2013). For the PRIMUS galaxies, we calculate SMFs after excluding one of the five target fields at a time. For the SDSS target galaxies we divide the field into a 12×9 rectangular RA and Dec grid and calculate the SMFs after excluding one grid at a time. From the calculated SMFs we calculate the uncertainty:

$$\sigma^j = \sqrt{\frac{N-1}{N}\sum_{k=1}^{M}(\Phi_k^j - \langle\Phi^j\rangle)^2} \qquad (5)$$

N in this equation is the number of jackknife SMFs in the stellar mass bin. $\langle\Phi^j\rangle$ is the mean number density of galaxies in each stellar mass bin for all of the jackknife Φ^js.

3.2. *Evolution of the Stellar Mass Function in Different Environments*

In Figure 3, we present the SMFs of the quiescent/star-forming (orange/blue, bottom/top panels) and high/low density environment (left/right panels) subsamples. The redshift evolution of the SMFs in each of these panels are indicated by a darker shade for lower redshift bins. The width of the SMFs represent the sample variance uncertainties derived in Section 3.1.

While a detailed comparison of the SMFs in each panel for different epochs is complicated by the different stellar mass completeness limits, we present some notable trends in each panel. In panel (a), star-forming galaxies in low density environments, we find a significant decrease in the high mass end of the SMF ($\mathcal{M} > 10^{10.75}\mathcal{M}_{\odot}$) over cosmic time. Meanwhile at lower masses ($\mathcal{M} < 10^{10.5}\mathcal{M}_{\odot}$), we observe no noticeable trend in the SMF. In panel (b), star-forming galaxies in high density environments, we do not observe any clear trends above the knee of the SMF ($\mathcal{M} \sim 10^{10.7}\mathcal{M}_{\odot}$) but an increase in SMF below the knee. For the quiescent population in low density environment, panel (c), we observe a potential decrease at higher masses ($\mathcal{M} > 10^{10.7}\mathcal{M}_{\odot}$). Lastly for the quiescent population in high density environments, panel (d), we find significant increase in Φ for lower masses but little trend at higher masses.

Observing the evolutionary trends in SMF for each of these sub-populations provides a narrative of the different galaxy evolutionary tracks involving environment and the end of star formation. For example, the decrease in the massive star-forming galaxies in low density environments over cosmic time can be attributed to the transition of those galaxies to any of the other panels. The star-forming galaxies in low density environments that have ended star formation over time are possibly responsible for the increase of the quiescent, low density environment SMF over time. The star-forming galaxies that fall into higher density environments explain the increase in the star-forming high density environment SMF below the knee. Finally, star-forming galaxies in high density environments that have ended their star-formation, quiescent galaxies that have transitioned from low to high density environments, and star-forming galaxies in low density environments that end their star-formation while infalling to high density environments all contribute to the overall increase of the high environment quiescent SMF.

In addition to the evolution over cosmic time, we observe noticeable trends when we compare the SMFs for star-forming and quiescent galaxies between the two environments. Comparison of the SMFs in low versus high density environments reveal a noticeable relation between mass and density, with SMFs in high density environments having more massive galaxies, especially evident in our lowest redshift bin. We further confirm this trend when we compare the median mass between the two environments to find that the median mass for galaxies in high density environments is significantly greater than in low density environments. The relationship between mass and environment observed in our SMFs reflects the well-established mass-density relation and observed mass segregation with environment in the literature (Norberg et al. 2002; Zehavi et al. 2002; Blanton et al. 2005a; Bundy et al. 2006; Scodeggio et al. 2009; Bolzonella et al. 2010).

While our mass complete subsample coupled with robust environment measurements allows us to compare SMF evolution for each of our subsamples out to $z = 0.8$, we caution readers regarding the photometric biases affecting the SDSS imaging (and perhaps the other imaging sources) and reserve detailed analysis of the SMFs for future investigation.

4. RESULTS: QUIESCENT FRACTION

The SMFs calculated in the previous section illustrate the stellar mass distribution of our galaxy population and its evolution over cosmic time. In this section, using the SMFs of our subsamples, we compare the quiescent and the star-forming populations by calculating the fraction of galaxies that have ended their star-formation, the quiescent fraction.

While the fractional relation of the star-forming and quiescent populations has been investigated in the past, with limited statistics, disentangling the environmental effects from underlying correlations among observable galaxy properties such as the color-mass or mass-density relations (Cooper et al. 2010) remains a challenge. With the better statistics available from SDSS and PRIMUS, we evaluate the quiescent fraction in bins of stellar mass, redshift, and environment in Section 4.1. By analyzing the quiescent fraction with respect to these properties, in Section 4.2 we explicitly compare the quiescent fraction evolution in low and high density environments. Our comparison reveal the subtle environmental effects on the quiescent fraction evolution. Furthermore, by quantifying this environmental effect, we are able constrain the role of environmental effects on how galaxies end their star formation.

4.1. *Evolution of the Quiescent Fraction*

From the SMF number densities (Φ) computed in the previous section, the quiescent fraction is computed as follows,

$$f_{\rm Q}(\mathcal{M}_*, z) = \frac{\Phi_Q}{\Phi_{SF} + \Phi_Q}. \quad (6)$$

Φ_Q and Φ_{SF} are the total number of galaxies per unit volume in stellar mass bin of $\Delta(\log \mathcal{M}) = 0.20$ dex for the quiescent and star-forming subsamples, respectively (Equation 4). We compute $f_{\rm Q}$ for high and low density environments for all redshift bins as plotted in Figure 4, which shows the evolution of $f_{\rm Q}$ for high (right panel) and low (left panel) density environments. As in Figure 3, the evolution of the quiescent fraction over cosmic time is represented in the shading (darker with lower redshift) and the uncertainty is represented by the width. For the uncertainty in the quiescent fraction, we use the standard jackknife technique, following the same steps as for the SMF uncertainty in Section 3.1.

Most noticeably in Figure 4, we find $f_{\rm Q}$ increases monotonically as a function of mass at all redshifts and environments. In other words, for galaxies in any environment since $z \sim 0.8$, galaxies with higher masses are more likely to have ceased their star-formation. With the roughly linear correlation between galaxy SFR to galaxy color and morphology, we find that this trend reflects the well established color-mass and morphology-mass relations: more massive galaxies are more likely to be red or early-type (Blanton & Moustakas 2009).

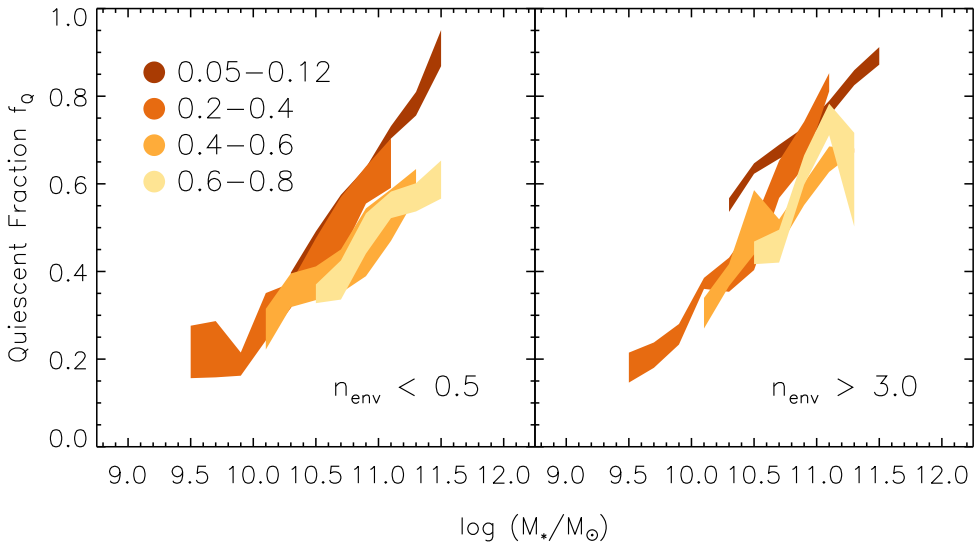

FIG. 4.— Evolution of the quiescent fraction f_Q for galaxies in low (left) and high (right) density environments for $z < 0.8$. f_Qs were calculated using the SMFs in Figure 3, as described in Section 4.1. Darker shading indicates lower redshift and the width represents the standard jackknife uncertainty.

Focusing on the redshift evolution of f_Q, we find that for both environments f_Q increases as redshift decreases. For high density environments, this is analogous to the Butcher-Oemler Effect (Butcher & Oemler 1984), which states that galaxy populations in groups or clusters have higher f_{blue} (lower f_Q) at higher redshift. This evolution occurs with roughly the same amplitude in low environments as well.

In addition, when we compare the stellar masses at which $f_Q = 0.5$ for each subsample, the so-called $\mathcal{M}_{50-50}$, we find that this quantity decreases over cosmic time. This corresponds to the well-known mass-downsizing pattern found by previous investigators (e.g. Bundy et al. 2006). Furthermore, the mass-downsizing trend observed in each of our environment subsample is qualitatively consistent with the trend observed in zCOSMOS Redshift Survey for isolated and group galaxies (Iovino et al. 2010).

Finally, we compare between our low and high density environment f_Qs at each redshift bin interval. For our lowest redshift bin, we find that f_Q at low density environments ranges from ~ 0.4 to ~ 0.9 for $10^{10.2}\mathcal{M}_\odot < \mathcal{M}_* < 10^{11.5}\mathcal{M}_\odot$. Over the same mass range, f_Q at high density environment ranges from ~ 0.55 to ~ 0.9. For our SDSS sample, f_Q in high density environments is notably higher.

For our PRIMUS sample at $z \sim 0.3$, over $10^{9.5}\mathcal{M}_\odot < \mathcal{M}_* < 10^{11}\mathcal{M}_\odot$ f_Q ranges from ~ 0.2 to ~ 0.65 for low density environment, while at high density environment f_Q ranges from ~ 0.2 to ~ 0.8. Similarly, at $z \sim 0.5$, over $10^{10}\mathcal{M}_\odot < \mathcal{M}_* < 10^{11.2}\mathcal{M}_\odot$ f_Q ranges from ~ 0.3 to ~ 0.6 for low density environment and f_Q ranges from ~ 0.3 to ~ 0.7. Finally in our highest redshift bin $z \sim 0.7$, over the mass range $10^{10.5}\mathcal{M}_\odot < \mathcal{M}_* < 10^{11.5}\mathcal{M}_\odot$, f_Q ranges from ~ 0.35 to ~ 0.6 for low density and ~ 0.45 to ~ 0.8 for high density. For the entire redshift range of our sample, f_Q in high density environment is higher than f_Q in low density environments.

TABLE 2
BEST FIT PARAMETERS FOR $f_Q(\mathcal{M}_*)$ FIT

$z_1 < z < z_2$	Environment	a	b
$0.05 < z < 0.12$	$n_{env} < 0.5$	0.410 ± 0.018	0.469 ± 0.007
	$n_{env} > 3.0$	0.270 ± 0.016	0.620 ± 0.008
$0.2 < z < 0.4$	$n_{env} < 0.5$	0.340 ± 0.032	0.432 ± 0.015
	$n_{env} > 3.0$	0.432 ± 0.018	0.544 ± 0.010
$0.4 < z < 0.6$	$n_{env} < 0.5$	0.263 ± 0.038	0.381 ± 0.018
	$n_{env} > 3.0$	0.289 ± 0.018	0.446 ± 0.013
$0.6 < z < 0.8$	$n_{env} < 0.5$	0.284 ± 0.036	0.352 ± 0.019
	$n_{env} > 3.0$	0.468 ± 0.065	0.429 ± 0.023

Notes: Best fit parameters in Equation 7 for each subsample $f_Q(\mathcal{M}_*)$ in Figure 4 for $\mathcal{M}_{fid} = 10^{10.5}\mathcal{M}_\odot$.

While there is a significant difference in f_Q between the environments, since the difference is observed from our highest redshift bin, it is not necessarily a result of environment dependent mechanisms for ending star formation. In order to isolate any environmental dependence, in the following section we quantitatively compare the evolution of the quiescent fraction between the different environments.

4.2. *Environmental Effects on the Quiescent Fraction Evolution*

In order to more quantitatively compare the f_Q evolution for different epochs and environments, we fit f_Q for each subsample to a power-law parameterization as a function of stellar mass,

$$f_Q(\mathcal{M}_*) = a \log\left(\frac{\mathcal{M}_*}{\mathcal{M}_{fid}}\right) + b, \quad (7)$$

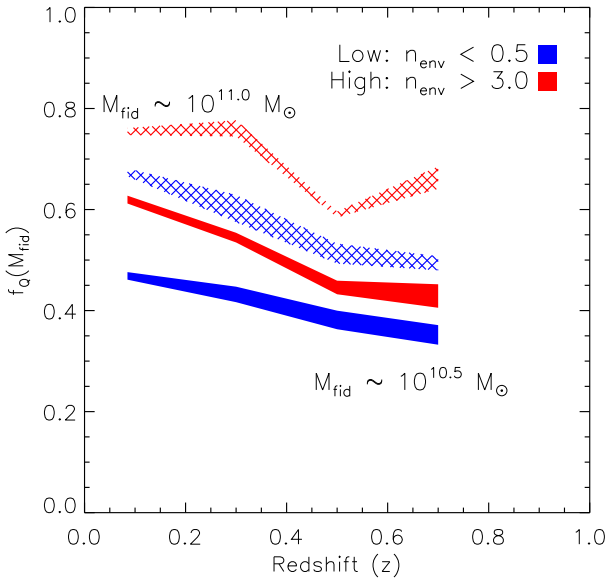

FIG. 5.— The evolution of the quiescent fraction at fiducial mass, $f_Q(\mathcal{M}_{\rm fid})$, for low (blue) and high (red) density environments within the redshift range $z = 0.0 - 0.8$. We present the $f_Q(\mathcal{M}_{\rm fid})$ evolution for $\mathcal{M}_{\rm fid} = 10^{10.5}\mathcal{M}_\odot$ (solid fill) and $10^{11}\mathcal{M}_\odot$ (patterned fill) with the uncertainty of the best-fit parameter b in Equation 7 represented by the width of the line. While the high density $f_Q(\mathcal{M}_{\rm fid})$ is greater than low density environment $f_Q(\mathcal{M}_{\rm fid})$ over the entire redshift range of our sample, there is a significant increase in $f_Q(\mathcal{M}_{\rm fid})$ over cosmic time for both environments. For the environment cut-offs ($n_{\rm env} < 0.5$ for low and $n_{\rm env} > 3.0$ for high), there is no significant difference in the slope of the evolution between the environments.

where a and b are best-fit parameters using *MPFIT* (Markwardt 2009) and $\mathcal{M}_{\rm fid}$ represents the empirically selected fiducial mass within the stellar mass limits where there is a sufficiently large number of galaxies. We primarily focus on $\mathcal{M}_{\rm fid} = 10^{10.5}\,\mathcal{M}_\odot$.

In Figure 5 we present the evolution of $f_Q(\mathcal{M}_{\rm fid})$ from $z \sim 0.7$ to ~ 0.1 at low (blue) and high (red) density environments for $\mathcal{M}_{\rm fid} = 10^{10.5}\,\mathcal{M}_\odot$ (solid fill) and $10^{11}\,\mathcal{M}_\odot$ (pattern fill). The width of the evolution represents the uncertainty derived from *MPFIT*. As noted earlier in Section 4.1, f_Q in high density environments is significantly greater than f_Q in low density environments for both fiducial mass choices. Throughout our sample's redshift range $f_Q(\mathcal{M}_{\rm fid})_{\rm high} - f_Q(\mathcal{M}_{\rm fid})_{\rm low} \sim 0.1$.

In addition, the $f_Q(\mathcal{M}_{\rm fid})$ evolution illustrates that the quiescent fraction in low density environment increases over cosmic time: $f_Q(\mathcal{M}_{\rm fid}, z \sim 0.1) - f_Q(\mathcal{M}_{\rm fid}, z \sim 0.7) \sim 0.1$. This significant quiescent fraction evolution for low density environments suggests that internal mechanisms, independent of environment, are responsible for a significant amount of star-formation cessation. Meanwhile, the $f_Q(\mathcal{M}_{\rm fid})$ evolution in high density environment ($f_Q(\mathcal{M}_{\rm fid}, z \sim 0.1) - f_Q(\mathcal{M}_{\rm fid}, z \sim 0.7) \sim 0.12$) shows little additional evolution.

When we increase our choice of $\mathcal{M}_{\rm fid}$ to $10^{11}\mathcal{M}_\odot$, aside from an overall shift in $f_Q(\mathcal{M}_{\rm fid})$ by ~ 0.2, we observe the same evolutionary trends. $f_Q(\mathcal{M}_{\rm fid} = 10^{11}\mathcal{M}_\odot)$ for both low and high density environments each increase by ~ 0.2 from at all redshifts we study. Increasing the fiducial mass to $10^{11}\mathcal{M}_\odot$ does not significantly alter the evolutionary trends in either environment. Although the varying stellar mass completeness at each redshift bin limits the masses we probe for the f_Q evolution, our f_Q evolution exhibits little mass dependence.

Because our fixed aperture definition of environment is susceptible to contamination due to PRIMUS redshift errors, we consider in Figure 6 more stringent high density environment classifications, extending the cut off to $n_{\rm env} > 5$ and 7 (specified in the top right legend and represented by the color of the shading). Aside from the increase in uncertainties that accompany the decrease in sample size of the purer high environment sample, we find an extension of the f_Q difference between the environments we stated earlier. A more stringent high environment classification significantly increases the overall $f_Q(\mathcal{M}_{\rm fid})$, which rises monotonically with the $n_{\rm env}$ limit.

More importantly, a purer high environment classification reveals a more significant environment dependence on the f_Q evolution. While the difference between the f_Q evolution in low and high density environment is negligible for the $n_{\rm env} > 3$ cut-off, there is a notable difference in f_Q evolution between our highest cut-off $n_{\rm env} > 7$ and our low density environment. $f_Q(\mathcal{M}_{\rm fid}, z \sim 0.1) - f_Q(\mathcal{M}_{\rm fid}, z \sim 0.7) \sim 0.25$ for $n_{\rm env} > 7$ versus $f_Q(\mathcal{M}_{\rm fid}, z \sim 0.1) - f_Q(\mathcal{M}_{\rm fid}, z \sim 0.7) \sim 0.1$ for low density environment. In addition to the environment independent internal mechanisms that can explain the f_Q evolution in low density environments, there may be other environment dependent mechanisms that can account for the moderate environment dependence of the f_Q evolution. Our measured difference in the f_Q evolution between environments provides an important constraint for any environmental models for ending star formation.

4.3. *Comparison to Literature*

Although a direct comparison with other results is difficult due to our sample specific methodology, a number of results from the literature have investigated the quiescent fraction in comparable fashions. In this section we compare our f_Q results from above to a number of these results, specifically from SDSS and zCOSMOS, with similarly defined samples and analogous environment classifications.

In Figure 6, we plot best-fit parameterization of $f_{\rm red}$ for high and low density environment from SDSS (panel a), zCOSMOS (panel b), and Peng et al. (2010) (filled square; panel d) from both surveys. From Iovino et al. (2010) (empty square; panel b), we calculate $f_{\rm red} = 1 - f_{\rm blue}$ using the best-fit $f_{\rm blue}$ from the mass bin $\mathcal{M} = 10^{10.3} - 10^{10.8}\mathcal{M}_\odot$. From Kovač et al. (2014) (triangle; panel b) we plot an estimated f_Q by applying the residual between SFR based and color based galaxy classifications to the best-fit $f_{\rm red}$ at $\mathcal{M} = 10^{10.5}\mathcal{M}_\odot$ for low ($\delta = 0.0$) and high density environments ($\delta = 1.5$). Similarly, from Baldry et al. (2006) (diamond; panel a) we plot f_Q derived from the best-fit $f_{\rm red}$ at $\mathcal{M} = 10^{10.5}\mathcal{M}_\odot$ for low ($\delta = 0.0$) and high density environment ($\delta = 1.0$). For Geha et al. (2012) (cross; panel a), we plot f_Q for their isolated galaxy sample in their mass bin closest to $10^{10.5}\mathcal{M}_\odot$, $\mathcal{M} = 10^{10.55}\mathcal{M}_\odot$. Finally for Peng et al. (2010) (square; panel c), we plot the parameterized $f_{\rm red}$ at $\mathcal{M} = 10^{10.5}\mathcal{M}_\odot$ using their best-fit parameters for low

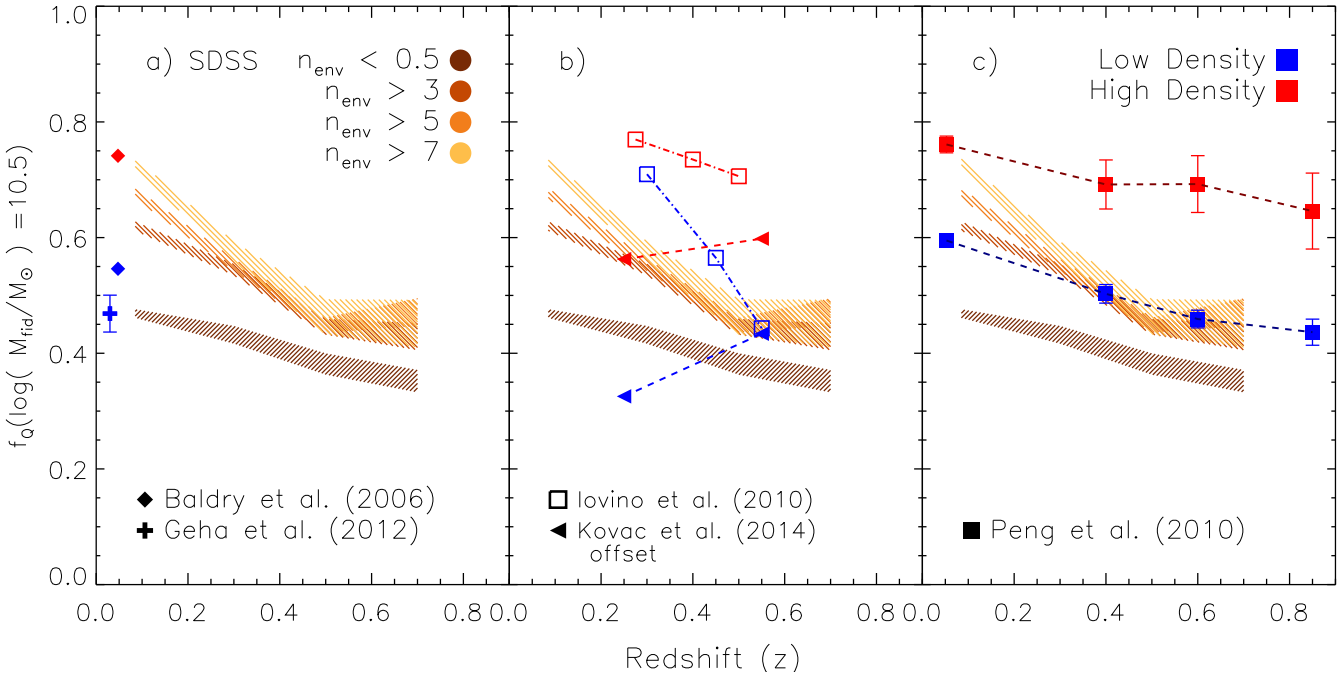

FIG. 6.— $f_{\rm Q}(\mathcal{M}_{\rm fid} = 10^{10.5}\mathcal{M}_{\odot})$ evolution compared to $f_{\rm red}(\mathcal{M}_{*} \sim 10^{10.5}\ \mathcal{M}_{\odot})$ in the literature: Baldry et al. (2006) (diamond) and Geha et al. (2012) (cross) from SDSS (panel a), Iovino et al. (2010) (empty square) and Kovač et al. (2014) (triangle) from zCOSMOS (panel b), and Peng et al. (2010) from both SDSS and zCOSMOS (panel c). The $f_{\rm red}$ values from Iovino et al. (2010), Kovač et al. (2014), Baldry et al. (2006), and Peng et al. (2010) are calculated from the best-fit parameterizations presented in the respective works. High density environment is represented in red and low density environment is represented in blue. The $f_{\rm Q}$ value from Geha et al. (2012) is the $f_{\rm Q}$ value at $\mathcal{M} = 10^{10.55}\mathcal{M}_{\odot}$. Uncertainties in the Iovino et al. (2010) best-fit $f_{\rm red}$ is omitted due to insufficient information on the cross correlation terms of the fit parameters. For Kovač et al. (2014) we apply the offset between the color-based and SFR-based galaxy classification in order to plot the $f_{\rm Q}$ estimates. We also plot the $f_{\rm Q}(\mathcal{M}_{\rm fid} = 10^{10.5}\mathcal{M}_{\odot})$ evolution of our sample with varying environment cut-offs specified on the top right. As in Figure 5 the width of the $f_{\rm Q}(\mathcal{M}_{\rm fid} = 10^{10.5}\mathcal{M}_{\odot})$ evolution represent the uncertainty in the best-fit parameters of Equation 7.

($\delta = 0.0$) and high ($\delta = 1.4$) density environments.

For our lowest redshift bin SDSS sample, we find that our $f_{\rm Q}$ for low and high environments are consistent with other SDSS $f_{\rm Q}$ (or $f_{\rm red}$) measurements as a function of environment. For example, Baldry et al. (2006) uses projected neighbor density environment measures ($\log\ \Sigma$) to obtain $f_{\rm Q}(\mathcal{M})$ for a range of environmental densities. Although the different environment measurements make direct comparisons difficult, in their corresponding higher environments ($\log\ \Sigma > 0.2$ in Baldry et al. 2006) $f_{\rm Q}(\mathcal{M} \sim 10^{10.2}\mathcal{M}_{\odot}) \sim 0.6$ and $f_{\rm Q}(\mathcal{M} \sim 10^{11.5}\mathcal{M}_{\odot}) \sim 0.9$, which is in agreement with our high density environment. Likewise, for lower environments ($\log\ \Sigma < -0.4$ in Baldry et al. 2006) $f_{\rm Q}(\mathcal{M} \sim 10^{10.2}\mathcal{M}_{\odot}) \sim 0.4$ and $f_{\rm Q}(\mathcal{M} \sim 10^{11.5}\mathcal{M}_{\odot}) \sim 0.8$, which also agree with our low density environment $f_{\rm Q}$. The Baldry et al. (2006) points (diamond) in Figure 6 reflect this agreement.

More recently, Tinker et al. (2011), using a group-finding algorithm on the SDSS DR7, presents the relationship between $f_{\rm Q}$ and overdensity for galaxies within the mass range $\log\ \mathcal{M} = [9.8, 10.1]$. The Tinker et al. (2011) $f_{\rm Q}$ at the lowest and highest overdensities, $f_{\rm Q} \sim 0.4$ and $f_{\rm Q} \sim 0.6$ respectively, are consistent with our $f_{\rm Q}$ for low and high density environment at the lower mass limit ($\log\ \mathcal{M} \sim 10.2$).

A modified Tinker et al. (2011) sample is used in Geha et al. (2012) to obtain $f_{\rm Q}$ for isolated galaxies over a wider mass range ($10^{7.4}\mathcal{M}_{\odot}$ to $10^{11.2}\mathcal{M}_{\odot}$). Although Geha et al. (2012) probe a slightly lower redshift range ($z \leq 0.06$), their $f_{\rm Q}$ is consistent with our low density sample. Within the overlapping mass range, at the low mass end Geha et al. (2012) find $f_{\rm Q}(\mathcal{M}_{*} \sim 10^{10.2}\mathcal{M}_{\odot}) \sim 0.3$ and at the high mass end they find $f_{\rm Q}(\mathcal{M}_{*} \sim 10^{11.2}\mathcal{M}_{\odot}) \sim 0.8$. Both of these values agree with our lowest redshift $f_{\rm Q}$ results in low density environment. Figure 6 illustrates the $f_{\rm Q}$ agreement for $\mathcal{M}_{*} = 10^{10.5}\mathcal{M}_{\odot}$.

For $z > 0.2$, we compare our PRIMUS $f_{\rm Q}$ results to the $f_{\rm red}$ (or $1 - f_{\rm blue}$) results from the zCOSMOS Redshift Survey (Iovino et al. 2010; Kovač et al. 2014), which covers a similar redshift range as PRIMUS. Iovino et al. (2010), and Kovač et al. (2014) using a mass-complete galaxy sample derived from zCOSMOS and a group catalog, 3D local density contrast, and overdensity environment measurements, respectively, compare $f_{\rm red}$ with respect to environment. The $f_{\rm blue}$ for group and isolated galaxies from Iovino et al. (2010) are generally inconsistent with our $1 - f_{\rm Q}$ for high and low density environments.

Similarly, $f_{\rm red}$ for high and low overdensities in Kovač et al. (2014) are greater overall than the PRIMUS $f_{\rm Q}$ values in high and low density environments. However, Kovač et al. (2014) points out that there is a significant difference between classifying the quiescent population using color and SFR due to dust-reddening in star-forming galaxies. For their lower redshift bin ($0.1 < z <$

0.4) Kovač et al. (2014) find that their $f_{\rm Q}$ defined by color is greater than $f_{\rm Q}$ defined by SFR by roughly 0.2. While for their higher redshift bin ($0.4 < z < 0.7$) the difference is $0.15 - 0.19$. Although Kovač et al. (2014) does not elaborate on how the galaxy classification discrepancy applies to the different environments, if we simply account for the difference uniformly for $f_{\rm red}$ at all environments, the Kovač et al. (2014) results in their lower redshift bin are roughly consistent with our $f_{\rm Q}$ at high and low density environments. Even accounting for the dust-reddening of $f_{\rm red}$, Kovač et al. (2014) finds a significantly higher $f_{\rm Q}$ in their higher redshift bin.

In Figure 4, the $f_{\rm Q}$ evolution with respect to mass reveals, qualitatively, little mass dependence in the evolution. Moreover, in Figure 5, we illustrated that adjusting the fiducial mass only shifted the overall $f_{\rm Q}(\mathcal{M}_{\rm fid})$, but did not change the $f_{\rm Q}$ evolutionary trend. The consistency in the $f_{\rm Q}$ evolutionary trends over change in fiducial mass suggests that $f_{\rm Q}$ evolution exhibit little mass dependence within the mass range probed in our analysis. In contrast to the weak mass dependence we observe in our results, Iovino et al. (2010) find significantly different $f_{\rm Q}$ evolution at $\mathcal{M} \sim 10^{11}\mathcal{M}_{\odot}$ and $\mathcal{M} \sim 10^{10.5}\mathcal{M}_{\odot}$, for both group and isolated galaxies. In fact at their highest mass bin ($10^{10.9} - 10^{11.4}\mathcal{M}_{\odot}$), Iovino et al. (2010) find no evolution for both environments: constant $f_{\rm blue} \sim 0.1$ over $z = 0.3 - 0.8$ for both group and isolated galaxy populations.

Meanwhile in their mass bin most comparable to $\mathcal{M}_{\rm fid} \sim 10^{10.5}\mathcal{M}_{\odot}$ ($10^{10.3}\mathcal{M}_{\odot} - 10^{10.8}\mathcal{M}_{\odot}$), Iovino et al. (2010) finds that $f_{\rm blue}$ evolves by ~ 0.1 from $z = 0.5$ to 0.25 for group galaxies and by ~ 0.3 from $z = 0.55$ to 0.3 for isolated galaxies as presented in panel (b) of Figure 6. Altogether, with mass bins beyond the fiducial masses we explore, Iovino et al. (2010) find a strong mass dependence with $f_{\rm Q}$ evolving significantly more in lower mass bins. While our sample from PRIMUS provides larger statistics than zCOSMOS, the mass-completeness limits we impose on our sample limits the mass range we probe (e.g. $\mathcal{M} > 10^{10.5}\mathcal{M}_{\odot}$ for our $z \sim 0.7$ bin). Consequently our results cannot rule out mass dependence in the $f_{\rm Q}$ evolution at lower masses.

In Figure 5 and Figure 6 we quantified that throughout our redshift range, high density environments have a significantly greater $f_{\rm Q}(\mathcal{M}_{\rm fid})$ than the low density environments. This finding is in agreement with the zCOSMOS results from Cucciati et al. (2010) and Kovač et al. (2014). As illustrated in panel (b) of Figure 6, Kovač et al. (2014) finds $f_{\rm Q}$ in high density environment significantly greater than $f_{\rm Q}$ at low density environment. Moreover, since galaxy color serves as a proxy for SFR, our results support the existence of the color-density relation (Cucciati et al. 2010; Cooper et al. 2010) and is not consistent with the color-density relation being merely a reflection of the mass-density relationship, as Scodeggio et al. (2009) suggest it is based on the Vimos VLT Deep Survey ($0.2 < z < 1.4$).

In Section 4.2, we showed that $f_{\rm Q}$ in low density environments evolves over cosmic time. From this trend we deduce that internal, environment independent, mechanisms contribute to ending star-formation in galaxy evolution. Iovino et al. (2010) from zCOSMOS, plotted in Figure 6 panel (b), also find that $f_{\rm Q}$ in low density environment increases with decreasing redshift. On the other hand Kovač et al. (2014), also from zCOSMOS, presents that $f_{\rm Q}$ in low density environment decreases over cosmic time. While the uncertainties for the parameterized $f_{\rm Q}$ are not listed, and thus not shown in Figure 6, once they are accounted for, Kovač et al. (2014) find no significant $f_{\rm Q}$ evolution over cosmic time. However, once we account for the dust-reddening of the $f_{\rm red}$, we find a more significant decrease over cosmic time (Figure 6 panel b).

Furthermore, in Section 4.2, our comparison of the $f_{\rm Q}$ evolution between the lowest density environment and the highest density environment revealed a modicum of evidence for the existence of environment dependent mechanisms. The same comparison with zCOSMOS results (Iovino et al. 2010; Kovač et al. 2014) present trends inconsistent with our findings. First, comparing the high (red) and low (blue) density environments for Iovino et al. (2010) in Figure 6 shows that there are indeed pronounced discrepancies between the $f_{\rm Q}$ evolution in different environments. Group galaxies in Iovino et al. (2010) have higher overall $f_{\rm Q}$ than isolated galaxies. However, unlike our results, which find a greater $f_{\rm Q}$ evolution at higher density environments, Iovino et al. (2010) finds the opposite environment dependence that there is a significantly greater $f_{\rm Q}$ evolution for isolated galaxies.

Next, Kovač et al. (2014) also find that overall $f_{\rm Q}$ is greater in high density than in low density environments. Like their low density environment $f_{\rm Q}$ evolution, $f_{\rm Q}$ in high density environment decreases over cosmic time between their two redshift bins. Although the decrease in $f_{\rm Q}$ over cosmic time conflicts with our results, Kovač et al. (2014) finds a greater (less negative) $f_{\rm Q}$ evolution in high density environments relative to low density environments, suggesting an environment dependence that is in the same direction as our results. We note that the negative slopes of the $f_{\rm Q}$ evolution in both environments are enhanced in Figure 6 due to the dust-reddening correction we impose to the Kovač et al. (2014) $f_{\rm red}$ results.

While the zCOSMOS survey provides more precise spectroscopic redshifts than PRIMUS, our sample provides significantly larger statistics. In addition, our sample covers a larger portion of the sky. Our SDSS-*GALEX* sample covers $2,505$ deg^2. More comparably, our PRIMUS sample covers 5.5 deg^2, over 3 times the sky coverage of zCOSMOS (1.7 deg^2). Furthermore, our PRIMUS sample is constructed from five independent fields which allows us to significantly reduce the effects of cosmic variance.

As listed in Table 1, after our edge effect cuts and stellar mass completeness limits, our sample consists of $13,734$ galaxies from PRIMUS over $0.2 < z < 0.8$ and $63,417$ galaxies from SDSS over $0.05 < z < 0.12$. Meanwhile, Iovino et al. (2010) has 914 galaxies with $\mathcal{M} > 10^{10.3}\mathcal{M}_{\odot}$ over $0.1 < z < 0.6$ and 1033 galaxies with $\mathcal{M} > 10^{10.6}\mathcal{M}_{\odot}$ over $0.1 < z < 0.8$. For the actual sample used to obtain the best-fit $f_{\rm Q}$ values in Figure 6 Iovino et al. (2010) has 617 galaxies. In comparison, our PRIMUS sample alone contains > 20 times the number of galaxies. While there is a considerable difference in the overall $f_{\rm Q}$ between our results and those of Iovino et al. (2010), the use of different methodologies, particularly

for galaxy classification and environment measurements, make such comparisons ambiguous. On the other hand, the discrepancies in the $f_{\rm Q}$ evolutionary trends with our results may be explained by the limited statistics in the Iovino et al. (2010) sample.

The more recent Kovač et al. (2014) provides larger statistics with $2,340$ galaxies in their lower redshift bin ($0.1 < z < 0.4$) and $2,448$ galaxies in their higher redshift bin ($0.4 < z < 0.7$). Although their sample is smaller than the PRIMUS sample, which contains over twice times the number of galaxies, the Kovač et al. (2014) sample provides a more stable comparison. Once their results are adjusted for the dust-reddening, we find that their overall $f_{\rm Q}$ is more or less consistent with our overall $f_{\rm Q}$. However, it is difficult to explain the significant discrepancies in the $f_{\rm Q}$ evolutionary trends. The significant overdenities observed in the COSMOS field at $z \sim 0.35$ and $z \sim 0.7$ (Lilly et al. 2009; Kovač et al. 2010) may have a significant effect on the zCOSMOS results and offer a possible explanation for the discrepancies.

5. SUMMARY AND DISCUSSION

Using a stellar mass complete galaxy sample derived from SDSS and PRIMUS accompanied by a consistently measured galaxy environment from robust spectroscopic redshifts, we measure the stellar mass functions for star-forming and quiescent galaxies in low and high density environments over the redshift range $0.05 < z < 0.8$. From these stellar mass functions, we compare the proportion of galaxies that have ended their star-formation within the subsamples by computing the quiescent fraction for each of them. In order to better quantify the evolution of the quiescent fraction over cosmic time, we fit our quiescent fraction anchored at a fiducial mass.

From our analyses we find the following notable results. The first three demonstrate that previous findings that are well known in the local universe are applicable out to $z \sim 0.7$. The last two are consistent with the findings of Peng et al. (2010) but provide increased detail on the environmental dependence of galaxy evolution:

1. From the SMFs, we find that the galaxy population in high density environments, both star-forming and quiescent, have a higher median mass, thus confirming the mass-density relation and mass-segregation in different environments throughout our sample's redshift range.

2. For all subsamples, $f_{\rm Q}$ increases monotonically with galaxy stellar mass, showing a clear mass dependence and reflecting the well-established color-mass and morphology-mass relations.

3. We illustrate that $f_{\rm Q}$ in high density environments is greater than $f_{\rm Q}$ in low density environments regardless of mass and out to redshift $z \sim 0.7$. This result reflects the well known trend that galaxies in high density environment are statistically redder, have lower SFRs, and are more massive.

4. $f_{\rm Q}$ increases significantly with redshift for both low and high density environments. For high density environment, this trend is the Butcher-Oemler effect. Furthermore, the $f_{\rm Q}$ evolution in low density environment suggest the existence of internal environment-independent mechanisms for ending star formation.

5. Comparison of the $f_{\rm Q}(\mathcal{M}_{\rm fid})$ evolution for a range of environment classifications reveals that the since $z = 0.8$, $f_{\rm Q}$ has evolved by a greater amount in the highest density environments. For our purest high environment sample ($n_{\rm env} > 7$), the total $f_{\rm Q}$ evolution is ~ 0.1 greater than the total $f_{\rm Q}$ evolution in low density environment, revealing a moderate dependence on environment.

Many physical mechanisms have been proposed to explain the cessation of star-formation observed in many galaxies. Recently star-formation cessation has often been classified into internal or external mechanisms, and sometimes more specifically into mass-dependent and environment-dependent mechanisms (Baldry et al. 2006; Peng et al. 2010). The significant redshift evolution of the $f_{\rm Q}$ in low density environments confirms the existence of internal mechanisms that end star-forming in galaxies.

Furthermore, the greater $f_{\rm Q}$ evolution in the highest density environment relative to low density environments suggests that in addition to the internal mechanisms, in high density environments such as groups and clusters, environment-dependent effects may also contribute to the end of star-formation. Our results do not specifically shed light on which mechanisms (e.g. strangulation, ram-pressure stripping, etc.) occur in high density environments. Not to mention, the mechanism could yet be indirect; for example, the galaxies in higher density environments could end star-formation primarily due internal processes, which affect the galaxies that end up in groups and clusters more greatly. Nevertheless, our results impose important constraints on the total possible contribution of environment dependent mechanisms that models must satisfy, providing a limit on the role of environment in ending star formation in galaxies.

CH and MB were supported by NSF-AST-1109432 and NSF-AST-0908354. MB was also supported by NSF-AST-1211644. ALC acknowledges support from NSF CAREER award. We acknowledge Katarina Kovač and Ying-Jie Peng for insightful discussions. We also thank Marla Geha for providing published quiescent fraction results in electronic format.

Funding for PRIMUS has been provided by NSF grants AST-0607701, 0908246, 0908442, 0908354, and NASA grant 08-ADP08-0019. The Galaxy Evolution Explorer (GALEX) is a NASA Small Explorer, launched in April 2003, whose mission was developed in cooperation with the Centre National d'Etudes Spatiales of France and the Korean Ministry of Science and Technology. Funding for the SDSS and SDSS-II has been provided by the Alfred P. Sloan Foundation, the Participating Institutions, the National Science Foundation, the U.S. Department of Energy, the National Aeronautics and Space Administration, the Japanese Monbukagakusho, the Max Planck Society, and the Higher Education Funding Council for England. The SDSS Web Site is http://www.sdss.org. The SDSS is managed by the Astrophysical Research Consortium for the Participating Institutions.

REFERENCES

Abazajian, K. N., Adelman-McCarthy, J. K., Agüeros, M. A., et al. 2009, ApJS, 182, 543
Baldry, I. K., Balogh, M. L., Bower, R. G., et al. 2006, MNRAS, 373, 469
Baldry, I. K., Glazebrook, K., & Driver, S. P. 2008, MNRAS, 388, 945
Balogh, M. L., Navarro, J. F., & Morris, S. L. 2000, ApJ, 540, 113
Behroozi, P. S., Marchesini, D., Wechsler, R. H., et al. 2013, ApJ, 777, L10
Bekki, K. 2009, MNRAS, 399, 2221
Bell, E. F., Wolf, C., Meisenheimer, K., et al. 2004, ApJ, 608, 752
Bell, E. F., Papovich, C., Wolf, C., et al. 2005, ApJ, 625, 23
Bernardi, M., Hyde, J. B., Sheth, R. K., Miller, C. J., & Nichol, R. C. 2007, AJ, 133, 1741
Blanton, M. R., Eisenstein, D., Hogg, D. W., & Zehavi, I. 2006, ApJ, 645, 977
Blanton, M. R., Kazin, E., Muna, D., Weaver, B. A., & Price-Whelan, A. 2011, AJ, 142, 31
Blanton, M. R., Lupton, R. H., Schlegel, D. J., et al. 2005a, ApJ, 631, 208
Blanton, M. R., & Moustakas, J. 2009, ARA&A, 47, 159
Blanton, M. R., & Roweis, S. 2007, AJ, 133, 734
Blanton, M. R., Schlegel, D. J., Strauss, M. A., et al. 2005b, AJ, 129, 2562
Bolzonella, M., Kovač, K., Pozzetti, L., et al. 2010, A&A, 524, A76
Borch, A., Meisenheimer, K., Bell, E. F., et al. 2006, A&A, 453, 869
Bundy, K., Ellis, R. S., Conselice, C. J., et al. 2006, ApJ, 651, 120
Butcher, H., & Oemler, Jr., A. 1984, ApJ, 285, 426
Chabrier, G. 2003, PASP, 115, 763
Coil, A. L., Blanton, M. R., Burles, S. M., et al. 2011, ApJ, 741, 8
Conroy, C., & Gunn, J. E. 2010, FSPS: Flexible Stellar Population Synthesis, astrophysics Source Code Library, ascl:1010.043
Cool, R. J., Moustakas, J., Blanton, M. R., et al. 2013, ApJ, 767, 118
Cooper, M. C., Newman, J. A., Madgwick, D. S., et al. 2005, ApJ, 634, 833
Cooper, M. C., Newman, J. A., Weiner, B. J., et al. 2008, MNRAS, 383, 1058
Cooper, M. C., Coil, A. L., Gerke, B. F., et al. 2010, MNRAS, 409, 337
Croton, D. J., Springel, V., White, S. D. M., et al. 2006, MNRAS, 365, 11
Cucciati, O., Iovino, A., Kovač, K., et al. 2010, A&A, 524, A2
Dekel, A., & Birnboim, Y. 2008, MNRAS, 383, 119
Desai, V., Dalcanton, J. J., Aragón-Salamanca, A., et al. 2007, ApJ, 660, 1151
Dressler, A. 1980, ApJ, 236, 351
Dressler, A. 1984, ARA&A, 22, 185
Faber, S. M., Willmer, C. N. A., Wolf, C., et al. 2007, ApJ, 665, 265
Fasano, G., Poggianti, B. M., Couch, W. J., et al. 2000, ApJ, 542, 673
Gallazzi, A., Bell, E. F., Wolf, C., et al. 2009, ApJ, 690, 1883
Geha, M., Blanton, M. R., Yan, R., & Tinker, J. L. 2012, ApJ, 757, 85
Gunn, J. E., & Gott, III, J. R. 1972, ApJ, 176, 1
Guzzo, L., Strauss, M. A., Fisher, K. B., Giovanelli, R., & Haynes, M. P. 1997, ApJ, 489, 37
Hermit, S., Santiago, B. X., Lahav, O., et al. 1996, MNRAS, 283, 709
Hopkins, A. M., & Beacom, J. F. 2006, ApJ, 651, 142
Hubble, E. P. 1936, The Realm of the Nebulae (New Haven: Yale University Press)
Hyde, J. B., & Bernardi, M. 2009, MNRAS, 394, 1978
Iovino, A., Cucciati, O., Scodeggio, M., et al. 2010, A&A, 509, A40
Jarrett, T. H., Chester, T., Cutri, R., et al. 2000, AJ, 119, 2498
Johnston, R. 2011, A&A Rev., 19, 41
Karim, A., Schinnerer, E., Martínez-Sansigre, A., et al. 2011, ApJ, 730, 61
Kereš, D., Katz, N., Weinberg, D. H., & Davé, R. 2005, MNRAS, 363, 2
Kovač, K., Lilly, S. J., Cucciati, O., et al. 2010, ApJ, 708, 505
Kovač, K., Lilly, S. J., Knobel, C., et al. 2014, MNRAS, 438, 717
Larson, R. B., Tinsley, B. M., & Caldwell, C. N. 1980, ApJ, 237, 692
Lauer, T. R., Faber, S. M., Richstone, D., et al. 2007, ApJ, 662, 808
Leja, J., van Dokkum, P., & Franx, M. 2013, ApJ, 766, 33
Lilly, S. J., Le Brun, V., Maier, C., et al. 2009, ApJS, 184, 218
Magnelli, B., Elbaz, D., Chary, R. R., et al. 2009, A&A, 496, 57
Markwardt, C. B. 2009, in Astronomical Society of the Pacific Conference Series, Vol. 411, Astronomical Data Analysis Software and Systems XVIII, ed. D. A. Bohlender, D. Durand, & P. Dowler, 251
Martin, D. C., Fanson, J., Schiminovich, D., et al. 2005, ApJ, 619, L1
Moore, B., Lake, G., & Katz, N. 1998, ApJ, 495, 139
Morrissey, P., Schiminovich, D., Barlow, T. A., et al. 2005, ApJ, 619, L7
Moustakas, J., Coil, A. L., Aird, J., et al. 2013, ApJ, 767, 50
Muldrew, S. I., Croton, D. J., Skibba, R. A., et al. 2012, MNRAS, 419, 2670
Noeske, K. G., Weiner, B. J., Faber, S. M., et al. 2007, ApJ, 660, L43
Norberg, P., et al. 2002, MNRAS, 332, 827
Oemler, A. 1974, ApJ, 194, 1
Peng, Y.-j., Lilly, S. J., Kovač, K., et al. 2010, ApJ, 721, 193
Pozzetti, L., Bolzonella, M., Zucca, E., et al. 2010, A&A, 523, A13
Salim, S., Rich, R. M., Charlot, S., et al. 2007, ApJS, 173, 267
Scodeggio, M., Vergani, D., Cucciati, O., et al. 2009, A&A, 501, 21
Skibba, R. A., Sheth, R. K., Croton, D. J., et al. 2013, MNRAS, 429, 458
Smith, G. P., Treu, T., Ellis, R. S., Moran, S. M., & Dressler, A. 2005, ApJ, 620, 78
Swanson, M. E. C., Tegmark, M., Hamilton, A. J. S., & Hill, J. C. 2008, MNRAS, 387, 1391
Taylor, E. N., Franx, M., van Dokkum, P. G., et al. 2009, ApJ, 694, 1171
Tinker, J., Wetzel, A., & Conroy, C. 2011, ArXiv e-prints, arXiv:1107.5046
Weinmann, S. M., van den Bosch, F. C., Yang, X., et al. 2006, MNRAS, 372, 1161
West, A. A. 2005, PhD thesis, University of Washington, Washington, USA
West, A. A., Garcia-Appadoo, D. A., Dalcanton, J. J., et al. 2010, ApJ, 139, 315
Williams, R. J., Quadri, R. F., Franx, M., van Dokkum, P., & Labbé, I. 2009, ApJ, 691, 1879
Wilman, D. J., Zibetti, S., & Budavári, T. 2010, MNRAS, 406, 1701
York, D. G., Adelman, J., Anderson, Jr., J. E., et al. 2000, AJ, 120, 1579
Zehavi, I., et al. 2002, ApJ, 571, 172